Proactive And Smooth Maneuvering For Navigation Around Pedestrians

Maria Kabtoul, Anne Spalanzani, Philippe Martinet

Proactive And Smooth Maneuvering For Navigation Around Pedestrians

Maria Kabtoul[1,2], Anne Spalanzani[1] and Philippe Martinet [2]

***Abstract*— Navigation in close proximity with pedestrians is a challenge on the way to fully automated vehicles. Pedestrian-friendly navigation requires an understanding of pedestrian reaction and intention. Merely safety based reactive systems can lead to sub-optimal navigation solutions resulting in the freezing of the vehicle in many scenarios. Moreover, a strictly reactive method can produce unnatural driving patterns which cannot guarantee the legibility or social acceptance of the automated vehicle. This work presents a proactive maneuvering method adapted to navigation in close interaction with pedestrians using a dynamic channel approach. The method allows to proactively explore the navigation options based on anticipating pedestrians cooperation. The navigation is tested in frontal and lateral crossing scenarios with variable space density. The system is implemented under ROS, and compared with the probabilistic Risk-RRT planning method. The results are evaluated based on the safety and comfort of the pedestrians, and the quality of the vehicle's trajectory.**

I. INTRODUCTION

Pedestrian populated environments present a unique challenge to autonomous vehicles navigation systems. The shared navigation space results in a coupled pedestrian-vehicle planning problem, where the navigation requires cooperation between the two parties. The stringent safety measures in such scenarios led to the development of strictly reactive navigation systems. In reactive methods the navigation space is explored and a path or a channel is selected among a set of obstacle free options based on an optimization criterion (shortest for example) [1]. However, ignoring the cooperation between the two parties can lead to the freezing of the vehicle and not just in highly dense spaces [2]. This problem can occur even with one human interactions if the agent is navigating in close proximity [3]. This makes the coupled behavior problem a central issue and not just a limit problem. This results in complex and non-convex planning objective functions. This computational complexity starts becoming obvious even in a simple collision avoidance cooperative objective, such as the one in [4] where the problem is tackled locally.

Therefore, different adaptations and proactive optimization criteria need to be formulated, to navigate around pedestrians in a natural, socially acceptable and safe manner. Furthermore, interpreting pedestrian behaviors and conveying a legible trajectory is essential for the success of this cooperative navigation task. Missing the legibility aspect in the navigation framework results in unpredictable or incomprehensible vehicle behaviors. This miscommunication prevents pedestrian cooperation, which leads to sub-optimal navigation solutions. To produce natural and legible vehicle trajectories, human-like navigation is often adapted. Many works discusses human-like navigation for autonomous vehicles driving in structured environments during different scenarios such as intersections, highways and lane change maneuvers for example [5],[6]. While unstructured environments do not impose strict driving roles, it remains beneficial to adapt such techniques, as any maneuver which does not resembles the driving patterns of experienced drivers is considered unnatural and illegible to pedestrians.

In this work, a proactive and natural maneuvering is suggested for navigation around pedestrians. The work implements a two-step method for the local steering of the vehicle. In a first step, the space is explored and dynamically divided into a set of channels using a local segment of the global path. The cost of navigating in each channel is computed and an optimal channel is found using a fuzzy cost model. The center line of the selected channel is then supplied as a goal path to the second layer of the local navigator to compute the steering controls. To convey a human-like steering behavior, a smooth lane change maneuver is adapted to travel between channels using a Quintic transition path [7]. In the final stage the exact tracking control commands are derived using a sliding mode control method [8].

The structure of this paper is as follows: In section II we give a background on the models used for both the vehicle and the pedestrians, as well as, the longitudinal velocity control method. Sections III and IV present the method of selecting the dynamic navigation channel and the design of the steering controller. Finally, section V presents the implementation of the method, the comparison with the Risk-RRT method and the discussion of the main simulation results.

II. BACKGROUND, TERMS AND NOTATIONS

Let (O, X_G, Y_G) be the global Cartesian Coordinates map frame. Two additional local coordinate frames are used in this work (Fig. 1). The first is the the vehicle's local Cartesian Coordinates frame $(O_R, \vec{X_V}, \vec{Y_V})$, where O_R is the center of the rear wheels axes and $\vec{x_V}$ is in the direction of the longitudinal velocity of the vehicle $\vec{v}$. The second local frame is a Frenet frame [9], which is defined by the tangential and normal vectors at a certain point of a reference curve. In the case of degenerate curves, the tangential is defined in parallel to the curve. In the following: the symbols X^g, X^v and $X^{\mathcal{F}_\mathbf{C}}$ denotes the coordinates of a point X expressed in the global frame, the vehicle frame and the Frenet frame of a curve $\mathbf{C}$ respectively.

[1]Univ. Grenoble Alpes, Inria, 38000 Grenoble, France
[2]Université Cote d'Azur, Inria, Sophia Antipolis, France

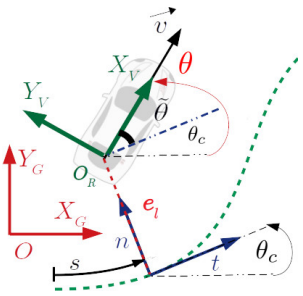

Fig. 1: The vehicle coordinate frames

Firstly, the vehicle model used in this work is the kinematic bicycle model with a zero slip assumption. This model is convenient since the navigation among pedestrians imposes low velocity and acceleration limits on the vehicle [10]. As shown in Fig. 1, the vehicle's model is defined in the Frenet frame of a path $\mathbf{C}$ using the the lateral displacement and the traveled arc length (e_l and s respectively), and the heading error angle between the vehicle and the tangential vector to the path: $\tilde{\theta} = \theta - \theta_C$. Assuming L is the wheelbase length of the vehicle, $\kappa(s)$ is the curvature of the path, δ is the steering control input and $\omega = \frac{v}{L}\tan(\delta)$. Then, the vehicle model can be written at O_R as follows [11]:

$$\dot{s} = v\cos(\tilde{\theta})\frac{1}{1 - e_l\kappa(s)} \qquad \dot{e_l} = v\sin(\tilde{\theta}) \quad (1)$$

$$\dot{\tilde{\theta}} = \omega - v\cos(\tilde{\theta})\frac{\kappa(s)}{1 - e_l\kappa(s)} \qquad \dot{v} = a \quad (2)$$

Given a longitudinal acceleration control input a provided by an external controller, and given a global path P_G provided by a higher level global planner; the problem of autonomous navigation is reduced to finding the steering angle of the vehicle $\delta \in [\delta_{min}, \delta_{max}]$.

Secondly, the model used to predict pedestrians behavior around the vehicle is the cooperation-based behavioral model presented in [12]. The model is constructed based on social rules and cognitive studies, and learnt using the observed behaviors in real-life recorded pedestrian-vehicle interactions. The model allows to estimate the tendency of an agent to cooperate with the vehicle in a given situation. his estimation is expressed by a time-varying scalar called the cooperation factor of the agent ($CF \in [0, 1]$), which will be used later in our algorithm.

Finally, the method used for the longitudinal control which provides the input a is the proactive longitudinal velocity controller presented in [13]. This method depends on computing an optimal proactive acceleration control a based on a trade-off between two criteria: reducing the social impact of the vehicle on the surrounding pedestrians, and increasing the pedestrians cooperation.

III. The Proactive Dynamic Channel (PDC)

Open and unstructured environments can lead to a large range of navigation options. Many of these options risk generating unnatural and illegible vehicle trajectories. The requirement of natural, legible and human-like driving is met in unstructured environments by imagining a local structure of the space. This imagined structure helps generating driving patterns similar to those of experienced road drivers. The proactive dynamic channel method is based on exploring a look-ahead navigation space of the vehicle and partitioning it to a set of possible navigation options (channels). This partitioning is based on a segment of the global path, which results in a local path modification. In the following we explore how a navigation channel is defined, how the space exploration occurs, and the way of selecting the optimal navigation option.

Let $\mathcal{D}_P \in \mathbb{R}_+$ be the perception range of the vehicle, then space perceived in the direction of the vehicle or the forward perception space $\mathbf{S}$ is:

$$\mathbf{S} = \{||X^v||_2 \leqslant \mathcal{D}_P; X^v \in (\mathbb{R}_+ \times \mathbb{R})\} \quad (3)$$

We call a channel every sub-space of $\mathbf{S}$ defined by a center point, width, length and orientation:

$$CH_i = \{(x_i, y_i), \theta_i, (W_i, L_i)\} \in \{\mathbb{R}^2, [0, 2\pi], \mathbb{R}^2_+\} \quad (4)$$

To partition the space $\mathbf{S}$ into a set of channels with a constant channel width W_C, then it can be divided into a set of K channels, where: $W_C K \leqslant 2\mathcal{D}_P$.
The partitioning of the space into a set of K channels is done based on the global path of the vehicle P_G (Fig. 2a). If p_j is the next waypoint on the global path, and (p_j, t, n) is the Frenet frame at this point ($\mathcal{F}_\mathbf{P}$). Then, the channels can be written in this Frame as:

$$CH_i^{\mathcal{F}_\mathbf{P}} = \{(\pm iW_C, 0), 0, W_C, L_C\}; i \in [0, nint(\frac{K}{2})] \quad (5)$$

where $nint(.)$ gives the nearest integer, and a constant width and length are set to all the channels. This operation is

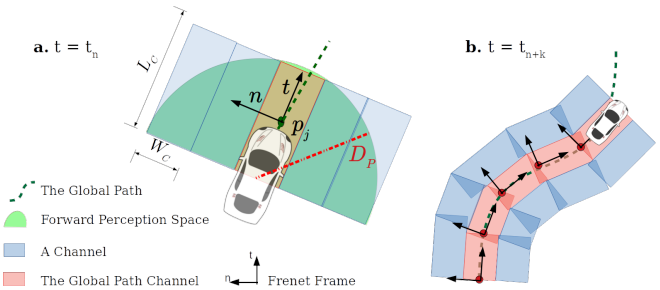

Fig. 2: Dynamic channels construction

repeated every time interval T_H. Therefore, the space is globally divided into a set of channels parallel to the global path. This is shown in Fig. 2b, where the overall channels sequence resulting after a number of iterations is visualized.

By computing the set of channels present in the navigation space, the task of finding a valid path is reduced to selecting the optimal navigation channel. This decision making step is essential in the proactive navigation framework, as it defines the general direction of the vehicle in the space. The navigation cost of each channel is evaluated by assigning a weight to each channel w_C. The higher the weight w_C the more costly is to navigate in this channel in terms of pedestrian discomfort and travel/time cost.

A. The navigation cost of a dynamic channel

The first navigation cost weight w_{state} is based on the state of the channel itself to minimize the discomfort caused to pedestrians navigation in the channel under evaluation. This criteria is necessary but not sufficient, as the navigation cost to a channel depends on the pose of the vehicle, it's goal or global path as well. To account for this cost, two additional channel cost weights are defined: the travel cost from the vehicle's current pose to the channel (w_{local}), and the travel cost from the channel back to the global path (w_{global}). This allows penalizing travelling far distances from the current position of the vehicle or from its reference global path, over minor advantages in terms of pedestrian discomfort.

Let $X_{CH}(t)$ be the center point of the channel, D_P the perception range, and $p_j(t)$ the next waypoint on the global path at time t. Then the local and global navigation costs, and final navigation cost to a channel C are written as:

$$w_{local}(t) = \frac{1}{2D_P}||X^v_{CH}(t)||_2 \in [0,1] \tag{6}$$

$$w_{global}(t) = \frac{1}{2D_P}||X^v_{CH}(t) - p^v_j(t)||_2 \in [0,1] \tag{7}$$

$$w_C(t) = \beta_0 \left[w_{state}(t) + \beta_1 w_{local}(t) + \beta_2 w_{global}(t)\right] \tag{8}$$

where: $\beta_k \in [0,1] \ : k \in \{0,1,2\}$. This formulation allows to select the channel with the optimal state while adding a penalty on travelling to further away channels. Therefore, distant channels are only selected if this selection results in a significant advantage in terms of the navigation cost.

Finally, the weight w_{state} is based on the state of pedestrians within the channel under evaluation. In the following, fuzzy logic [14] is used to construct a navigation cost weight model for w_{state}. This method is selected as it is efficient, tolerant to suboptimality or imprecision, and only needs a set of navigation rules based on experience.

B. The channel cost fuzzy model w_{state}

To comply with the principals of pedestrian safety and socially-aware navigation, channels with less pedestrians and/or more cooperative pedestrians should be preferred. Therefore, the first input used to estimate the channel state cost weight is the pedestrian density in a channel $D(t)$. The second input is the expected density change in the channel over a future navigation horizon T_H (ΔD). This change in density is found by predicting the pedestrians trajectories over T_H using the model in [12], then recomputing the resulting density at the end of the prediction time horizon. The third input is the percentage of uncooperative agents in the channel $N_{UC\%}$. Proactive navigation is a common task that requires cooperation between the pedestrians and the vehicle. This means that the navigation system should manoeuvre in directions containing more cooperative pedestrians who are willing to compromise their paths and facilitate the vehicle's navigation. These three model inputs are computed as follows:

$$D(t) = \frac{\pi R_p^2 M(t)}{L_C W_C}, \qquad N_{UC\%}(t) = \frac{M_{UC}(t)}{M(t)} \tag{9}$$

$$\Delta D(t) = D(t + T_H) - D(t) \tag{10}$$

with M the total number of pedestrians in the channel, R_p the personal space radius, and M_{UC} the number of agents with a low cooperation factor ($CF \leqslant 0.5$). The output of the fuzzy model is a channel weight $w_{state} \in [0,1]$.

Triangular functions are used as membership functions for both the inputs and the output. The fuzzy values assigned to each input are: $D \in \{High, Mid, Low\}$, $\Delta D \in \{Decrease, Static, Increase\}$ and $N_{UC\%} \in \{Low, High\}$. The model rules are constructed to prioritize channels with smaller weights. Therefore, lower weights are assigned to channels with lower densities, a decrease in their densities over the navigation horizon and/or a lower percentage of uncooperative pedestrians in the channel. The fuzzification and defuzzification of the values is done using the g-Fuzzification and the center of gravity methods respectively [14].

Finally, the channel with the least cost is selected as the goal channel. The task turns into transitioning to the selected channel and navigating within it, until a new channel is selected. In the following, we explore how the global path is modified locally to transition and navigate within the selected channels.

IV. Channel-Based Vehicle Maneuvering

Selecting a channel results in a goal navigation sub-space. To maintain a vehicle behavior similar to experienced drivers, a lane change maneuvering is adapted to perform the transition to the selected channel, as lane change maneuvering generates natural and legible vehicle trajectories.

Many techniques have been developed for the purpose of autonomous lane change. The first category of techniques is optimization methods which depend on a designed cost-function with a set of constraints, such as the vehicle kinematics and road dimensions [15]. However, the optimization problem in this case is multi-objective, non-convex with multiple nonlinear constraints. Therefore, a global optimal solution cannot always be found in real-time [7]. The second category is sampling-based methods [16]. These techniques can generate many additional candidate paths that are not feasible or do not fulfill the safety constraints when navigating in close interaction with pedestrians. Several works suggest constructing a lane-change candidate path analytically [17]. The latter method allows to join the goal channel, while guaranteeing the exact transition behavior at all times. For this reason, a Quintic spline candidate which can guarantee a C2-continuous path is used as a transition candidate.
Let X_{CH} be the center of the goal channel, and let $\mathcal{F}_{\mathcal{X}_{\mathcal{CH}}}$ be the Frenet frame with respect to the channel center line. Supposing the vehicle state in this frame is $(e_l, s, \tilde{\theta})$, then the transition Quintic path can be written as:

$$e_q(s) = a_5 s^5 + a_4 s^4 + a_3 s^3 + a_2 s^2 + a_1 s + a_0 \tag{11}$$

The parameters of this function ($a_i \in \mathbb{R} \ : i \in \{0, ..., 5\}$) can be easily derived by applying the motion constraints in (12), the only variable that needs to be chosen is the look-ahead

navigation horizon L_H (Fig. 3).

$$\begin{array}{lll} e_q(L) = e_0 & \dot{e_q}(L) = 0 & \ddot{e_q}(L) = 0 \\ e_q(L_H) = 0 & \dot{e_q}(L_H) = 0 & \ddot{e_q}(L_H) = 0 \end{array} \quad (12)$$

where e_0 is the initial lateral displacement of the vehicle to the goal channel.

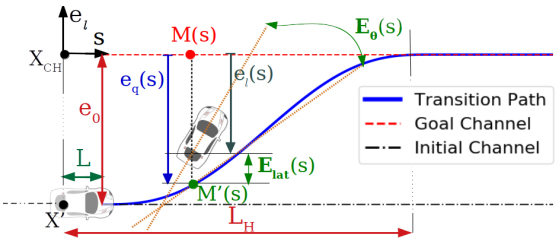

Fig. 3: Channel transition with the Quintic spline

Finally, the vehicle follows the integration of the channels center lines with the corresponding Quintic paths. Any appropriate path following technique can be integrated with this framework to produce the local steering commands. In the following we present the sliding-mode path follower developed in this work.

A. Local steering control: Path following

Several techniques are present in the literature for the purpose of path tracking [18]. These include MPC-based methods [19], learning-based methods [20] and other control theory methods such as sliding mode control (SMC) [8]. SMC is a nonlinear control technique that drives the target system to a designed surface in the state space, then keeps the system in a close neighborhood of this surface in a sliding (switching) manner. This method is selected to follow the previous Quintic spline during a channel transition as it is robust and easily implemented in real-time. Furthermore, the closed-loop performance becomes insensitive to system uncertainties [21]. The sliding mode steering controller is constructed using two tracking errors: the lateral displacement error and the heading error. This ensures the tracking of the path and the human-like maneuver while satisfying the smoothness in the vehicle heading as well. This can also contribute to the comfort of the vehicle's passengers. These two heading errors, as well as, the global tracking error can be written with respect to the vehicle model in the Frenet frame of the goal channel $\mathcal{F}_{\mathcal{X}_{\mathcal{CH}}}$ as follows:

$$E_{lat}(s) = e_l(s) - e_q(s), \qquad E_\theta(s) = \tilde{\theta}(s) \quad (13)$$

$$E(s) = E_{Lat}(s) + d_s E_\theta(s) \qquad : d_s \in \mathbb{R}^*_+ \quad (14)$$

To derive these errors, the closest point to the goal channel center line is found (M on Fig. 3). Then, the projection of this point on the Quintic (point M') is determined. Finally, the lateral displacement and the tangent to the Quintic are computed at M' to derive the lateral and heading errors.

To perform the tracking and since the relative in-out degree of our system is two, a first degree sliding surface is σ selected:

$$\sigma = \left(\frac{d}{dt} + \lambda\right) E(s) \quad (15)$$

where $\lambda \in \mathbb{R}^*_+$ defines the unique pole of the reduced dynamics system resulting in the closed loop. The control required to reach the goal state ($E(s) = 0, \dot{E}(s) = 0$) is composed of two parts. These two modes are an equilibrium control which drives the system to the sliding surface (δ_{eq}), and a sliding control δ_s (Fig. 4). The sliding control part keeps the system close to the sliding surface until the goal state is reached. The equilibrium control is achieved when σ is constant: $\delta_{eq} = \delta|_{\dot{\sigma}=0}$. This is solved by substituting the error derivatives in (14) and by using the vehicle's state space model $(\dot{s}, \dot{e_l}, \dot{\tilde{\theta}})$. With a zero-curvature assumption for the center channel path and by assuming small steering variations $\dot{\delta} \ll 1$, the equilibrium control is derived as a function of the state variables, and the control parameters:

$$\begin{array}{c} \delta_{eq} = F(\tilde{\theta}, s, v, a, \lambda, d_s, L, L_H, e_0) \\ F : [0, 2\pi] \times \mathbb{R}^{*8} \rightarrow [-\delta_m, \delta_m], \quad \delta_m = \frac{\pi}{6} \end{array} \quad (16)$$

Secondly, to find δ_s while avoiding the chattering phenomena which occurs in simpler first order SMC, we use the "Super Twisting" second order algorithm [22] which is a nonlinear version of the classic PI controller. Finally, given an initial state of the vehicle (s, e_l, θ, v, a) and a goal channel C, the sliding control and the total steering control are: with: $\gamma_1 =$

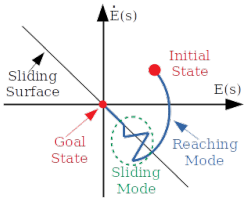

$$\delta_s = -\gamma_1 \sqrt{|\sigma|} sign(\sigma) + u \quad (17)$$

$$\text{with: } \dot{u} = -\gamma_0 sign(\sigma) \quad (18)$$

$$\delta = \delta_{eq} + \delta_s \quad (19)$$

Fig. 4: The sliding surface and the control modes in SMC

$U, \gamma_0 = 1.1U$, where $U \in \mathcal{R}_+$ is a constant to be tuned.

V. Simulations and Results

The navigation is tested using the PedSim simulator presented in [23] under ROS. Fig. 5 shows the information flow in the proactive dynamic channel maneuvering system wen implemented within the global navigation framework.

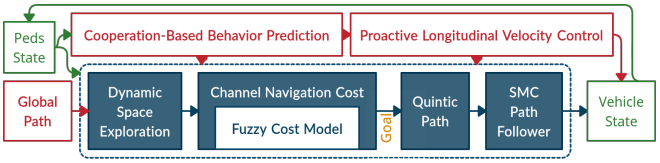

Fig. 5: The overall proactive maneuvering system

The method is tested in frontal and lateral crossing with a range of different average pedestrian density and distribution in the space. The pedestrian density is measured as the average number of pedestrians in the space, over the number of possible pedestrians occupying a 100% of the space.

A. Performance measures

The method is evaluated using four performance measures. The first is a qualitative measure used to evaluate the quality

of the vehicle's trajectory. This is done by evaluating the *smoothness of vehicle's path* using a path energy measure [24]. Let $X_j = (x_j, y_j)\ j \in [0, .., M]$ be the overall path of the vehicle during the simulation, then the equivalent path energy is evaluated as:

$$E_T = \frac{1}{M} \sum_{j=1}^{M} \left(\frac{y_j - y_{j-1}}{x_j - x_{j-1}} \right)^2 \tag{20}$$

where $E_T \in \mathcal{R}_+$ increases when a path contains more frequent and sharp maneuvers ($E_T = 0$ for a straight path).

Secondly, to evaluate the *pedestrian comfort* during the interaction with the vehicle, the uncomfortableness index ($\bar{I}_{ucf}$) suggested in [25] is used. This index is a qualitative measure which reflects the degree and frequency of the velocity change a pedestrian can experience during the interaction:

$$\bar{I}_{ucf} = \frac{1}{N} \sum_{i=1}^{N} \frac{\bar{y}_i}{\bar{h}_i} \tag{21}$$

where N is the total number of pedestrians in the simulation, $\bar{h}_i = \frac{1}{T_F} \sum_{t=t_0}^{t_0+T_F} v_i^2(t)$ and $\bar{y}_i = \frac{1}{T_F} \sum_{t=t_0}^{t_0+T_F} (v_i(t) - \bar{g}_i)^2$ are the mean square velocity and the deviation of the average velocity of agent i respectively. Whereas, $\bar{g}_i = \frac{1}{T_F} \sum_{t=t_0}^{t_0+T_H} v_i(t)$ the average velocity of agent i over the simulation period $[t_0, t_0 + T_F]$.

Finally, the *safety* of the navigation is quantitatively evaluated by measuring the collisions rate, and the average vehicle collision speed.

B. Parameters calibration

The steering controller parameters: the first parameter to tuned is the lookahead distance used to define the transition Quintic spline in (12). The lookahead distance is computed depending on the speed of the vehicle: $L_H = vK_F$ where $K_F = 10$. Fig. 6b shows the closed-loop system (path and steering) response with different values of K_F, which is selected to achieve a fast closed-loop response with minimal overshooting ($< 5\%$). The rest of the steering control parameters are tuned in a similar manner to achieve a smooth steering and avoid trajectory overshooting. The weight between the lateral and heading tracking errors in (14) is selected as $d_s = 2$. While the sliding surface constant in (15) is set to $\lambda = 10$. Finally, the "Super-twisting" parameter in (19) is tuned to $U = 10$.

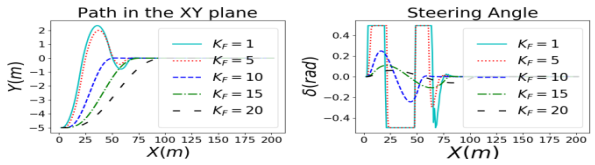

Fig. 6: Tuning the lookahead distance factor

To calibrate the **channel dimensions**, three performance measures are used: the travel time of the vehicle to reach its goal, it's path energy, and the uncomfortableness index. Firstly, a group of 540 simulations are ran to study the effect of the channel length on the performance. The following parameters are constant across all simulations: $v_{max} = 4m/s, T_F = 60s, W_C = 3m$. The simulations are grouped based on the density and the channel length, each group containing 30 simulations where six different channel lengths in $L_C \in [5, 120]m$ are tested. Secondly, different width values of the channels are tested in a similar manner to the previous test. Another group of 540 simulations are ran using the same previous configuration with a fixed channel length of $L_C = 40m$ and four different width value in $W_C \in [1, 10]m$. Fig. 7 shows the results of the three performance measures with the different channel lengths, widths and the three levels of density. Each point on the graph represents the average value for one group of simulations. The results show that larger channel lengths reduce the vehicle travel time and increase the comfort of pedestrians. Moreover, larger channel lengths significantly reduce the vehicle's path energy resulting in smoother trajectories with less channel change along the simulation. This is a result of anticipating a larger space horizon to plan and select the best maneuvering option. However, the relationship between the channel length and it's effect on the navigation is not linear. The results show that a minimum channel length is required to obtain a high performance gain. This minimum length is equal to around $20m$ in our case. Whereas, increasing the length beyond that limit results in smaller performance gains. Moreover, large loss in efficiency in terms of the travel time and pedestrian comfort occurs when using a large channel width. On the other hand, a large channel width results in a more smooth path as less partitions of the space are explored thus resulting in less steering options. Finally, a channel length and width of $40m$ and $1m$, respectively, are selected to maintain a smooth path while maximizing pedestrian comfort and minimizing the vehicle travel time.

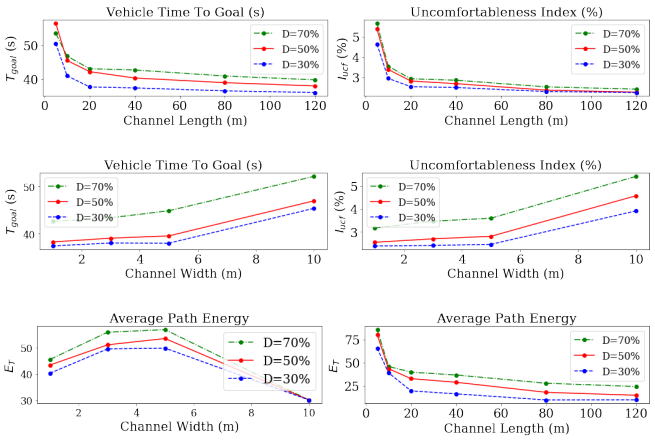

Fig. 7: Effect of changing the channel dimensions

C. Tests results

A total of 840 simulations are ran (520 frontal and 320 lateral) with over $10K$ pedestrian trajectories. The simulations included pedestrian crowds with average density ranging between $D \in [20, 90]\%$. The maximum speed of the vehicle, the simulation duration and the channel width/length are constant across all the simulations ($v_{max} = 4m/s, T_F =$

$60s, W = 1m, L = 40m$ respectively). Fig. 8 shows three examples of the resulting paths in the XY plane. Even though the dynamic channels are straight locally, the vehicle path does not have zero curvature globally. As shown in Fig. 8, the resulting paths are different smooth curves depending on the particular interaction.

Moreover, the same tests are ran using the Risk Rapidly-exploring Random Trees or **Risk-RRT** method. This method improves the classic RRT by integrating a risk assessment of potential collisions [26]. The method is selected as a reference for comparison, as the proposed probabilistic framework is designed for navigation in dynamic environments.

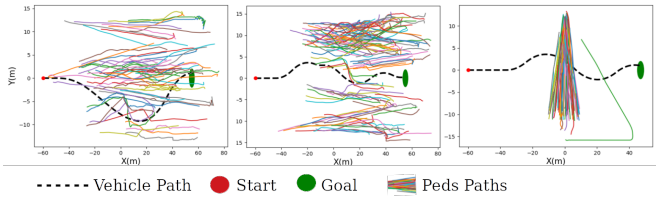

Fig. 8: Resulting paths in three interaction tests.

Table I shows the results in both the lateral and frontal scenarios for our method (PDC) and the Risk-RRT method. Firstly, the results of the collisions tests are shown for the **pedestrian safety** analysis. Additionally, the **success rate** for each method is shown, which is the percentage of simulations where the vehicle reached its goal destination within the simulation period. There is a significant improvement in terms of the navigation success (in both scenarios) when using the proactive framework. The Risk-RRT method is noticed to fail in planning a trajectory in many interaction scenarios due to its reactive and uncooperative nature. The vehicle was noted to freeze in many cases, specially with higher densities. Whereas, using the suggested PDC method, the vehicle anticipates the pedestrian cooperation and succeeds to find a valid solution. This is done while maintaining a better pedestrian safety than the Risk-RRT. In the PDC, the vehicle was adapting its behavior in critical situation resulting in no frontal collisions and low collision speed. Moreover, a low collision rate is detected in the frontal crossing coupled with a high success rate. In the lateral crossing, a slightly higher collision rate is detected in our method.

Secondly, the study in [27] is used as a reference to analyze the pedestrians comfort in the test simulations. The study evaluated $\bar{I}_{ucf}$ using pedestrian trajectories recorded at a crossing area in Japan. For the **pedestrian comfort**, in both scenarios our values for $\bar{I}_{ucf}$ fall under the limits of the reference values, which shows that the method guarantees a similar level of pedestrian comfort around the vehicle, to the level of comfort experienced in daily pedestrian interactions. However, the values in the lateral crossing scenarios are twice as more than the frontal crossing scenarios. For the **path smoothness**, in our method E_T falls in a low energy range, which shows that the smooth steering adapted in our method allowed to produce smooth trajectories in both the frontal and lateral interactions. The Risk-RRT freezes in many cases, which results in a very low path energy. Moreover, in frontal crossing the vehicle in Risk-RRT was not adapting its trajectory according to pedestrian cooperation which resulted in lower levels of pedestrian comfort than our method.

Finally, in the lateral crossing for Risk-RRT, a slightly lower collision rate and lower pedestrian uncomfortableness are detected. However, this result is coupled with a very low success rate ($< 10\%$) which means that the vehicle, in most cases, did not succeed to insert itself in the pedestrian crowd.

Collisions Test					Success Rate
Method		Rate	Speed	Type	
PDC	Frontal	**0.0057**	**0.25m/s**	Side	**98%**
	Lateral	0.32	**0.65m/s**	Side	**78%**
Risk-RRT	Frontal	0.01	$3.13m/s$	Side/Front	22%
	Lateral	**0.31**	$2.36m/s$	Side/Front	8.3%
		$\bar{I}_{ucf}$ (%)		E_T (%)	
Method		Mean	Max	Mean	Max
Reference	All	7.39	29.2		
PDC	Frontal	**3.07**	**5.37**	1.85	5.32
	Lateral	6.46	10.31	1.60	4.95
Risk-RRT	Frontal	4.32	6.86	0.18	1.5
	Lateral	**5.64**	**8.78**	0.08	0.48

TABLE I: Pedestrians Safety and Comfort Results

VI. Conclusion

This work presented a local maneuvering technique adapted to autonomous vehicles navigation in shared spaces with pedestrians. The method was tested using the PedSim simulator under ROS and compared with the Risk-RRT method. The test simulations included frontal and lateral crossing interactions between a vehicle and a group of pedestrians. The performance was evaluated based on pedestrian safety and comfort. The values of the pedestrian comfort indexes were compared against the values of a reference study of pedestrian comfort. The suggested navigation system managed to maintain the minimum required pedestrian comfort in the reference study, while maintaining a good safety level and a high success rate as compared to the reactive Risk-RRT method. However, our results showed a limitation in the method during lateral crossing interactions. During these interactions pedestrians experienced higher levels of uncomfortableness and side collisions. This is a limitation that will be addressed in future work. Furthermore, the generated vehicle's path was analyzed and qualified using a path smoothness measure. The results showed that smooth trajectories are produced while exploring further navigation options, and limiting the steering effort.

The scope of this work was limited to testing the maneuvering method with two interaction scenarios. Our future work will seek to generalize the method to more complex interaction scenarios.

Acknowledgment

This research is part of the HIANIC project, funded by the French National Research Agency (ANR-17-CE22-0010).

REFERENCES

[1] C. Cao, P. Trautman, and S. Iba, "Dynamic channel: A planning framework for crowd navigation," *CoRR*, vol. 143, 2019.

[2] P. Trautman and A. Krause, "Unfreezing the robot: Navigation in dense, interacting crowds," in *2010 IEEE/RSJ International Conference on Intelligent Robots and Systems*, 2010, pp. 797–803.

[3] C. I. Mavrogiannis, F. Baldini, A. Wang, D. Zhao, P. Trautman, A. Steinfeld, and J. Oh, "Core challenges of social robot navigation: A survey," *CoRR*, vol. abs/2103.05668, 2021.

[4] P. Trautman and K. Patel, "Real time crowd navigation from first principles of probability theory," in *Proceedings of the Thirtieth International Conference on Automated Planning and Scheduling, Nancy, France, October 26-30, 2020*, J. C. Beck, O. Buffet, J. Hoffmann, E. Karpas, and S. Sohrabi, Eds. AAAI Press, 2020, pp. 459–468. [Online]. Available: https://aaai.org/ojs/index.php/ICAPS/article/view/6741

[5] S. Gim, S. Lee, and L. Adouane, "Safe and efficient lane change maneuver for obstacle avoidance inspired from human driving pattern," *IEEE Transactions on Intelligent Transportation Systems*, pp. 1–15, 2020.

[6] D. S. González, M. Garzón, J. S. Dibangoye, and C. Laugier, "Human-like decision-making for automated driving in highways," in *IEEE Intelligent Transportation Systems Conference*, 2019, pp. 2087–2094.

[7] Z. Li, H. Liang, P. Zhao, S. Wang, and H. Zhu, "Efficent lane change path planning based on quintic spline for autonomous vehicles," in *2020 IEEE International Conference on Mechatronics and Automation (ICMA)*, 2020, pp. 338–344.

[8] C. Hwang, C. Yang, and J. Y. Hung, "Path tracking of an autonomous ground vehicle with different payloads by hierarchical improved fuzzy dynamic sliding-mode control," *IEEE Transactions on Fuzzy Systems*, vol. 26, no. 2, pp. 899–914, 2018.

[9] M. Frenet, "Sur les courbes à double courbure," *Toulouse. Abstract in Journal de Mathématiques Pures et Appliquées*, vol. 17, 1852.

[10] P. Polack, F. Altché, B. Novel, and A. de La Fortelle, "The kinematic bicycle model: A consistent model for planning feasible trajectories for autonomous vehicles?" in *IEEE Intelligent Vehicles Symposium*, Jun. 2017, pp. 812–818.

[11] C. Canudas de Wit, B. Siciliano, and G. Bastin, *Theory of Robot Control*. Springer Communications and Control Engineering, 1996.

[12] M. Kabtoul, A. Spalanzani, and P. Martinet, "Towards proactive navigation: A pedestrian-vehicle cooperation based behavioral model," *IEEE International Conference on Robotics and Automation. Virtual*, May 2020.

[13] M. Kabtoul, P. Martinet, and A. Spalanzani, "Proactive longitudinal velocity control in pedestrians-vehicle interaction scenarios," *IEEE Intelligent Transportation Systems Conference. Vritual*, Sep. 2020.

[14] T. J. Ross, *Fuzzy Logic with Engineering Applications, 4th Edition*. NJ: Wiley: Hoboken, Oct. 2016.

[15] Y. Zhong, L. Guo, Y. Zhang, Q. Liu, and H. Chen, "Optimal lane change control of intelligent vehicle based on mpc," in *2019 Chinese Control And Decision Conference (CCDC)*, 2019, pp. 1468–1473.

[16] D. Zeng, Z. Yu, L. Xiong, J. Zhao, P. Zhang, Z. Li, Z. Fu, J. Yao, and Y. Zhou, "A novel robust lane change trajectory planning method for autonomous vehicle," in *2019 IEEE Intelligent Vehicles Symposium (IV)*, 2019, pp. 486–493.

[17] T. Heil, A. Lange, and S. Cramer, "Adaptive and efficient lane change path planning for automated vehicles," in *2016 IEEE 19th International Conference on Intelligent Transportation Systems (ITSC)*, 2016, pp. 479–484.

[18] S. Dominguez, A. Ali, G. Garcia, and P. Martinet, "Comparison of lateral controllers for autonomous vehicle: Experimental results," in *2016 IEEE 19th International Conference on Intelligent Transportation Systems (ITSC)*, 2016, pp. 1418–1423.

[19] H. Ye, H. Jiang, S. Ma, B. Tang, and L. Wahab, "Linear model predictive control of automatic parking path tracking with soft constraints," *International Journal of Advanced Robotic Systems*, vol. 16, no. 3, 2019.

[20] J. Liu, Z. Huang, X. Xu, X. Zhang, S. Sun, and D. Li, "Multi-kernel online reinforcement learning for path tracking control of intelligent vehicles," *IEEE Transactions on Systems, Man, and Cybernetics: Systems*, pp. 1–14, 2020.

[21] G. Bartolini, L. Fridman, A. Pisano, and E. E. Usai, *Modern Sliding Mode Control Theory*. Springer Lecture Notes in Control and Information Sciences, Apr. 2018, vol. 375.

[22] A. Swikir and V. Utkin, "Chattering analysis of conventional and super twisting sliding mode control algorithm," in *2016 14th International Workshop on Variable Structure Systems (VSS)*, 2016, pp. 98–102.

[23] M. Prédhumeau, L. Mancheva, J. Dugdale, and A. Spalanzani, "An agent-based model to predict pedestrians trajectories with an autonomous vehicle in shared spaces," *20th International Conference on Autonomous Agents and Multiagent Systems*, Jan. 2021.

[24] A. M. Bruckstein and A. N. Netravali, "On minimal energy trajectories," *Computer Vision, Graphics, and Image Processing*, vol. 49, no. 3, pp. 283–296, 1990.

[25] D. Helbing, P. Molnár, I. J. Farkas, and K. Bolay, "Self-organizing pedestrian movement," *Environment and Planning B: Planning and Design*, vol. 28, no. 3, pp. 361–383, 2001.

[26] C. Fulgenzi, A. Spalanzani, C. Laugier, and C. Tay, "Risk based motion planning and navigation in uncertain dynamic environment," Research Report, Oct. 2010. [Online]. Available: https://hal.inria.fr/inria-00526601

[27] K. Teknomo, "Microscopic pedestrian flow characteristics: Development of an image processing data collection and simulation model," *CoRR*, vol. 29, 2016.